

Dreamguider: Tuning Free Conditional Generation

Nithin Gopalakrishnan Nair[✉] and Vishal M Patel[✉]

Johns Hopkins University, Baltimore, Maryland 21218

{ngopala2, vpatel36}@jhu.edu

<http://www.springer.com/gp/computer-science/lncs>

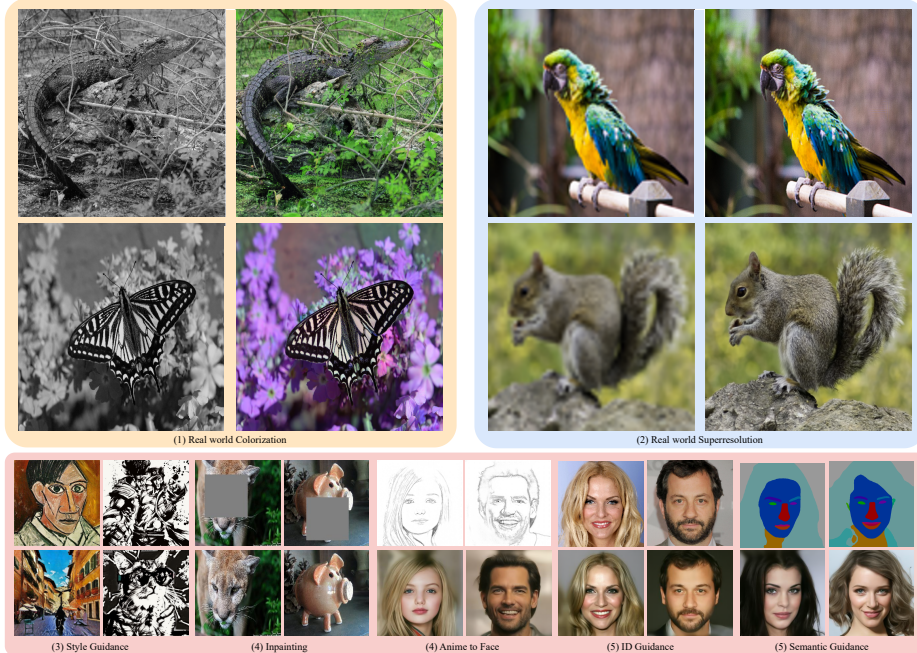


Fig. 1: An illustration of the different applications of our method. We utilize a pretrained diffusion model to generate images satisfying a predefined condition without any training, backpropagation through the diffusion UNet, or any hand-crafted parameter tuning. We present results on (1) Real-world colorization, (2) Real-world super-resolution, (3) Style-guided Text-to-Image Generation, (4) Inpainting, (5) Sketch-to-Face synthesis, (6) Face ID Guidance, and (7) Face Semantics-to-Face synthesis.

Abstract. Diffusion models have emerged as a formidable tool for training-free conditional generation. However, a key hurdle in inference-time guidance techniques is the need for compute-heavy backpropagation through the diffusion network for estimating the guidance direction. Moreover, these techniques often require handcrafted parameter tuning on a case-by-case basis. Although some recent works have introduced minimal compute methods for linear inverse problems, a generic lightweight guidance solution to both linear and non-linear guidance

problems is still missing. To this end, we propose Dreamguider, a method that enables inference-time guidance without the compute-heavy backpropagation through the diffusion network. The key idea is to approximate the guidance direction with respect to the current sample, thereby removing the backpropagation operation. Moreover, we propose an empirical guidance scale that works for a wide variety of tasks, hence removing the need for handcrafted parameter tuning. We further introduce an effective lightweight augmentation strategy that significantly boosts the performance during inference-time guidance. We present experiments using Dreamguider on multiple linear and non-linear tasks across multiple datasets and models to show the effectiveness of the proposed modules. To facilitate further research, we will make the code public.

Keywords: Diffusion models · Plug and Play Generation · Classifier guidance · Parameter-free Optimization

1 Introduction

Generative modeling utilizing Denoising Diffusion Probabilistic Models (DDPMs) [14, 19, 39, 43] has massively improved over the past few years. Multiple works have extended the use of diffusion models for text-to-image synthesis [3, 34, 36], 3D synthesis [22, 32], video generation [5, 18, 46], as well as for conditioning to solve inverse problems. Moreover, like conditional generative adversarial networks (GANs) [2, 15], DDPMs can be adapted to tasks based on a label [14, 34] or visual prior-based conditioning [35]. However, like conditional GANs [33, 44], DDPMs also need to be trained with annotated pairs of labels and instructions for satisfactory results. This poses a limitation in many cases where there is a lack of paired data to train large diffusion models. Due to this reason, there has been recent interest in models that can perform conditional generation without the need for explicit training [6, 16, 30, 50].

Progressing towards this direction is prior research in plug-and-play models. First introduced in [30], the initial research on plug-and-play models [16, 30] enabled conditional sampling from GANs trained with unlabeled data. For this, a pre-trained classifier [20, 38] or a captioning model was used to estimate the deviation between the GAN-generated image and a given label, and based on this deviation, the GAN input noise was modulated until the generated sample satisfied the given text or class label. A similar approach that has been attempted for diffusion models to facilitate conditional sampling from unconditional diffusion models is Classifier guidance [14, 16], where a noise-robust classifier is trained along with the diffusion model to guide the sampling towards a particular direction. However, classifier guidance brings in the computational costs of training a classifier, which is often undesirable. Some recent works have performed conditional generation without explicit training for the condition by utilizing the implicit guidance capabilities of the diffusion model [4, 8, 9, 29, 50]. Diffusion posterior sampling (DPS) [9] proposed a technique of using an L_2 norm-based loss function to solve linear inverse problems using unconditional diffusion models. However, DPS often requires a large number of sampling steps for photorealistic results. Freedom [50], yet another work, proposed the use of general loss functions during sampling to achieve training-free conditional sampling. Some variants of DPS have also been proposed in the

literature [42]. All the aforementioned loss-guided posterior sampling techniques involve a guidance function at each timestep that requires backpropagation through the diffusion UNet. Recently, [17] proposed Manifold Preserving Guided Diffusion Models (MGD) that remove the need for backpropagating through the diffusion U-Net by performing a gradient descent with respect to the Minimum Mean Square Error (MMSE). Although MGD [17] works remarkably well for linear tasks that require more guidance towards the start of the guidance process, it may fail in some tasks where guidance happens earlier, for example, face semantics-to-image and sketch-to-image, where stronger guidance is required from a much earlier stage. Moreover, like [29, 50], MGD also requires a case-by-case handcrafted parameter. Hence, a generic lightweight method that works well for both linear and non-linear guidance functions is still missing. Moreover, the need to find a handcrafted guidance parameter on a case-by-case basis still remains an open challenge.

In this paper, we introduce a new framework that can adaptively perform zero-shot generation using diffusion models without the need for any manual intervention by the user. We found a rather simple fix to the problem during the initial timesteps of diffusion, i.e., by utilizing the gradient with respect to the diffusion output noise. Combined with the guidance with respect to the MMSE estimate, we found that the combination generalizes well to tasks that require guidance at very early stages of guidance. Figure 2 presents the visualization of our approach over existing works present in the literature. Utilizing the correction term along with the correction with respect to the MMSE estimate significantly boosts the performance in non-linear tasks. We present the corresponding results in Section 6. Moreover, we treat the energy-based inference-time guidance [9, 50] as a stochastic gradient optimization of the MMSE estimate and the noise present in the image. This formulation enabled us to leverage recent research in parameter-free learning [11, 21] to develop a dynamic step size schedule. This step size adjusts itself adaptively based on the initial noise seed input of the diffusion model and guidance functions, hence removing the need for manual parameter tuning for inference-time guidance. Moreover, motivated by the effectiveness of differentiable augmentations while training GANs [53], we found that utilizing multiple levels of matching differentiable augmentations to the MMSE estimate and guidance reference significantly improves the sampling quality, enabling very high-quality sampling with a low number of guidance steps. We present an overview of the different applications of our method in Figure 1. Namely, we present results using Stable Diffusion [34], unconditional diffusion models released by [31] for 256×256 guidance, and class-conditional diffusion models for high-resolution 512×512 conditional synthesis. The different functionalities of Dreamguider are tabulated in Figure 2.

We present experiments on publicly released models on generic images, face images, and stable diffusion to show the relevance of our method. We focus on the tasks of (1) Inpainting, (2) Super-resolution, (3) Colorization, (4) Gaussian Deblurring, (5) Semantic label-to-image generation, (6) Face sketch-to-image, (7) ID guidance and identity generation, and beat existing benchmarks that utilize diffusion models for these tasks, obtaining a significant boost in performance over existing methods leveraging loss-guided models. To summarize, our contributions are:

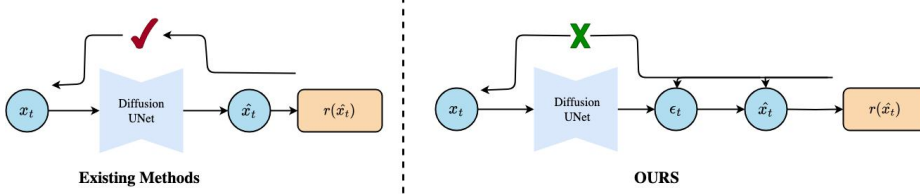


Fig. 2: An illustration of the difference between the existing method and our method. Existing works backpropagate through the diffusion network to perform guidance at each timestep, whereas we find the gradients with respect to the MMSE estimate and the predicted noise, thereby bypassing the expensive backpropagation operation.

- We propose a zeroth-order loss-guided diffusion guidance that is applicable to both linear inverse problems and non-linear inverse problems.
- We discover the need to optimize with respect to the diffusion model output noise.
- We remove the need for a manually tuned guidance scale for classifier guidance by proposing a scaling function that works for a wide variety of tasks.
- We propose a time-varying guidance scale for improving sampling quality.
- We propose a differentiable augmentation strategy to improve sampling quality.

2 Related Work

2.1 Training-free Conditional Sampling using Diffusion Models

Recently, there has been a rise in multiple works that propose utilizing unconditional diffusion models for conditional sampling [4, 10, 24, 29]. The earlier works proposed solving linear inverse problems using diffusion models with the help of priors dependent on the inverse transform of degradation. Recently, diffusion posterior sampling [9] considered the degradation to be conditioned on a Gaussian distribution given any intermediate timestep and derived an L_2 norm-based regularization at each intermediate timestep to solve for linear inverse problems. Recent works such as Freedom [50] explored an energy-based perspective and extended guidance to non-linear functions using general loss functions. Universal diffusion guidance [1] extended this guidance process to stable diffusion and improved the performance by using forward-backward guidance. More recent works, such as manifold-guided diffusion [17], further proposed to constrain the manifold space by projecting for the latent space alone. Steered diffusion [29] was proposed to guide the use of implicit prediction for non-linear functions, which utilized a hard constraint for normal functions and proposed a plug-and-play module to improve performance.

3 Background

3.1 Perturbed Markovian Kernel for Diffusion Transition

For conditional generation tasks using an unconditional diffusion model, ideally, the model would predict intermediates closer to the condition. Let us assume that $r(x_t, y)$

Table 1: Table illustrating the capabilities of Dreamguider over existing methods performing inference-time guidance

Method	Zeroth order	Linear Tasks	Non-Linear Tasks	Automatic scaling
DPS [8]	✗	✓	✗	✗
π GDM [41]	✗	✓	✗	✗
Freedom [50]	✗	✗	✓	✗
MGD [17]	✓	✓	✗	✗
OURS	✓	✓	✓	✓

gives a measure of the distance between an intermediate x_t and the condition y and is a positive bounded function. Hence, in the reverse process, the diffusion trajectory should proceed through distributions with a higher probability of being closer to the desired cases. We model these trajectory intermediate distributions with

$$\hat{p}(x_t) = p(x_t)r(x_t, y). \quad (1)$$

Dickenson et al. [39] first proposed the use of Markovian kernels to estimate the distribution of diffusion intermediates. Specifically, given the state x_t at the equilibrium of the training process for a diffusion model, the intermediate of a diffusion model at a time instant, the distribution at a timestep $t - 1$ can be estimated as

$$p(x_{t-1}) = \int p(x_t)p_\theta(x_{t-1}|x_t)dx_t. \quad (2)$$

As we know, the kernel $p(x_{t-1}|x_t)$ is a Gaussian distribution whose mean can be estimated using the diffusion UNet and x_t . To estimate a perturbed kernel $\hat{p}(x_{t-1}|x_t)$, the perturbed distribution can be modeled as

$$p(x_{t-1})r(x_{t-1}, y) = \int r(x_t, y)p(x_t)\hat{p}_\theta(x_{t-1}|x_t)dx_t. \quad (3)$$

By merging the constant terms in the transition into the normalization factor, the transition step can be modeled as

$$\hat{p}_\theta(x_{t-1}|x_t) = p_\theta(x_{t-1}|x_t)r(x_{t-1}, y). \quad (4)$$

The proof is given in the supplementary material. Hence, we can see that rather than considering a Gaussian posterior, as in DPS [9], any distance or loss function can be used. A similar idea was suggested in Steered Diffusion [29] also. Similarly, one other valid transition step of the perturbed process is

$$\hat{p}_\theta(x_{t-1}|x_t) = p_\theta(x_{t-1}|x_t)\frac{r(x_{t-1}, y)}{r(x_t, y)}, \quad (5)$$

which adopts the notion of reciprocal distance from the previous timestep.

3.2 Inference-time Guidance of Diffusion Models

The same formulation can also be seen in terms of transition probabilities. Consider a pretrained unconditional diffusion model on a specific domain. The problem at hand

needs to guide the diffusion model during inference time conditioned with a condition y . Dhariwal et al. [14] proposed a general strategy to perform this by conditioning on the condition y and finding the resultant marginal distribution

$$p(x_t|x_{t+1}, y) = p(x_t|x_{t+1})p(y|x_t). \quad (6)$$

By assuming the distribution $p(y|x_t)$ has much lower curvature compared to $p(x_t|x_{t+1})$, considering the marginal distribution close to x_t ,

$$\begin{aligned} \log p(y|x_t) &= (x_t - \mu) \nabla_{x_t} \log p(y|x_t), \\ g &= \nabla_{x_t} \log p(y|x_t). \end{aligned} \quad (7)$$

Plugging back to $\log(p(x_t|x_{t+1}, y))$,

$$\begin{aligned} \log(p(x_t|x_{t+1}, y)) &= (x - \mu - \Sigma g)^T \Sigma^{-1} (x - \mu - \Sigma g) + C, \\ p(x_t|x_{t+1}, y) &\sim N(\mu + \Sigma g, \Sigma). \end{aligned} \quad (8)$$

Hence, the reverse sampling equation becomes,

$$x_{t-1} = \frac{1}{\sqrt{\alpha_t}} \left(x_t - \frac{1 - \alpha_t}{\sqrt{1 - \alpha_t}} \epsilon_\theta(x_t) \right) + \sigma_t \epsilon + \Sigma \frac{dr(x_{t-1}, y)}{dx_{t-1}}, \epsilon \sim \mathcal{N}(0, I). \quad (9)$$

3.3 Shortcomings of the Existing Methods

Although the energy-based guidance theory supports guidance as a function of the current latent estimate, almost all loss-based guidance techniques derive the distance function as a function of x_t rather than x_{t-1} and derive the gradient based on the previous sample. Although this approach works for many tasks, it requires backpropagating through the neural network and modeling the score function for the guidance correction term. This limits the use of classifier guidance since existing diffusion architectures that produce photorealistic results are often very bulky. One can see why the existing framework utilizes the derivative with respect to the previous sample works by taking a better look at Equation (5). As we can see, a reciprocal distance over the previous timestep diffusion latent x_t is a perfectly valid distance guidance function. In the next section, we elaborate on Dreamguider.

4 Proposed Method

Suppose x_{t-1} denotes the current step and x_t denotes the previous step in the inference process of the diffusion module. As mentioned in the previous section, existing works utilize the derivative with respect to the previous step for guidance; one reason for this is to use an off-the-shelf auxiliary distance function on the MMSE estimate at each step \hat{x}_t , which enables the use of general functions defined on image space for guidance. Here, the MMSE estimate is defined as

$$\hat{x}_t = \frac{x_t - \sqrt{1 - \bar{\alpha}_t} \epsilon_\theta(x_t)}{\sqrt{\bar{\alpha}_t}}. \quad (10)$$

where $\bar{\alpha}$ denotes the variance schedule of the diffusion process and $\epsilon_\theta(x_t)$ is the noise estimated by the network. One other observation to note is that finding the derivative with respect to the current step requires finding \hat{x}_{t-1} , which again requires an additional propagation through the diffusion network. Hence, the dilemma of backpropagating through the UNet for guidance still remains unresolved.

We found a simple yet effective solution for this dilemma; if we take a look at the ODE estimate at each step proposed by Song et al. [40], we can see that in the extreme case of deterministic sampling, the next step can be decomposed as

$$x_{t-1} = \sqrt{\alpha_{t-1}}\hat{x}_t + \sqrt{1 - \alpha_{t-1}}\epsilon_\theta(x_t). \quad (11)$$

4.1 Double-Descent Classifier Guidance

Hence, rather than perturbing the Gaussian kernel at each timestep, we perturb the components \hat{x}_t and $\epsilon_\theta(x_t)$ by a small amount. Specifically, we perform the following operations:

$$\begin{aligned} \hat{x}_t &= \hat{x}_t - c\Sigma \frac{dr(\hat{x}_t, y)}{d\hat{x}_t} \\ \epsilon_\theta(x_t) &= \epsilon_\theta(x_t) - d\Sigma \frac{dr(\hat{x}_t, y)}{d\epsilon_\theta(x_t)} \\ x_{t-1} &= \frac{1}{\sqrt{\alpha_t}} \left(x_t - \frac{1 - \alpha_t}{\sqrt{1 - \bar{\alpha}_t}} \epsilon_\theta(x_t) \right) + \sigma_t \epsilon - c_t \Sigma \frac{dr(\hat{x}_t, y)}{d\hat{x}_t} - d_t \Sigma \frac{dr(\hat{x}_t, y)}{d\epsilon_\theta(x_t)}, \end{aligned} \quad (12)$$

Here $r(\hat{x}_t, y)$ is a non negative distance function that measures the distance between the MMSE estimate and condition, Σ is the variance of the latent estimate at each timestep as in Equation (8). Please note that we perform a double descent here; the intuition behind the double descent is that performing descent on one of the components, say \hat{x}_t , guides effectively at the end of the diffusion process where α_{t-1} is one and vice versa. During this descent, we treat the optimization problem like half quadratic splitting [51]. As we know, at any step \hat{x}_t and $\epsilon(x_t)$ are orthogonal. Hence, during the guidance with the gradient w.r.t \hat{x}_t , the maximum component of shift that happens to the sample is when we consider the flow of this correction through \hat{x}_t . Hence, we define the value as the maximum component of x_{t-1} present in \hat{x}_t .

$$c_t = c\sqrt{\alpha_{t-1}}. \quad (13)$$

Similarly, we define d_t as the maximal component of $\epsilon_\theta(x_t)$ in x_{t-1} . Hence,

$$d_t = -d \cdot \frac{1 - \alpha_t}{\sqrt{\alpha_t} \sqrt{1 - \bar{\alpha}_t}}. \quad (14)$$

Hence, this term gives efficient guidance at all timesteps, bypassing the guidance at the later timesteps alone as in MGD [17]. In the following section, we proceed to propose an effective empirical estimate for c and d that works for a wide range of tasks.

4.2 A Gradient-Dependent Scaling Factor Estimate

Recently, Distance over Gradients (DOG) [21] was proposed as an effective parameter-free dynamic step size schedule for SGD problems. According to DOG, given any Stochastic Gradient Descent (SGD) optimization problem, the Distance over Gradient works as an effective learning rate. Recent works [47] have found the diffusion process as a stochastic optimization problem and have derived an SGD-based interpretation of the diffusion sampling process. Hence, inspired by both of these works, we attempted an empirical guidance estimate of the form:

$$\gamma_t = \begin{cases} \frac{1e^{-5}}{\sqrt{g_T^2}}, & \text{if } t = T \\ \frac{\max_{i>t} |f_i - f_T|}{\sqrt{\sum_{i=t}^T g_i^2}}, & \text{otherwise} \end{cases} \quad (15)$$

where g_t is the gradient of the loss function as defined in the equation, f_t can be any of $\hat{x}_t, x_t, \epsilon_\theta(t)$ at timestep t and f_0 is the initial estimate of f_t . We noticed that this empirical estimate works well for first-order sampling involving DPS [9] as well. We illustrate more results on the effect of this plug-in value for different cases in the appendix. Hence, utilizing Equation (15), we estimate c and d accordingly by substituting f_i as \hat{x}_t and $\epsilon_\theta(x_t)$

4.3 Differential Augmentation Classifier Guidance

A common practice while performing classifier guidance to augment diffusion models with specific regularization for guidance is to use the noisy estimate at timestep t and utilize it to compute the loss function to regularize the current prediction. However, in many cases, such guidance can give results with artifacts and color shifts, as portrayed in Figure 3 and Figure 5, due to excessive guidance or insufficient guidance at intermediate timesteps that shift the results off manifold or cause color shifts. One effective solution for this is to imitate different versions of artifacts or color shifts on both the source image and the target image and utilize these augmented versions for a boost in performance. Hence, to perform guidance with a much more robust guidance loss, we introduce DiffuseAugment, an augmentation strategy for diffusion guidance during inference time. Specifically, given an intermediate sample x_t and condition y , we augment \hat{x}_t and y with differentiable augmentations denoted by

$$\hat{x}_t^{aug}, y^{aug} = T(\hat{x}_t^{aug}, y^{aug}). \quad (16)$$

We choose three different types of augmentations for T comprising random cutouts, random translations, and color saturations. Please note that the augmentation of y is dependent on the input signal. For label-based conditioning such as identity or text, we do not perform augmentation for y . For image space augmentations, we augment y with the same random augmentation as that of x . While computing the effective loss, we find the average across all augmentations. We find that DiffuseAugment significantly boosts the sampling fidelity and quality of the reconstructed image. We present these results in Section 6.

5 Experiments

Since our method comprises both linear and non-linear inverse tasks, for linear inverse tasks, we follow DPS and evaluate our method utilizing two different benchmarks: (1) ImageNet [12] and (2) CelebA [26]. For non-linear tasks, we follow Freedom and evaluate using the CelebA dataset. For linear tasks, we evaluate our method quantitatively for Super-resolution ($\times 4$), Colorization, Inpainting (Box), and Gaussian deblurring tasks. For non-linear tasks, we evaluate for Face Sketch guidance, Face Parse maps guidance, and Face ID guidance. Since our method falls into the category of loss-guided diffusion models, we perform all quantitative evaluations using existing methods that follow this kind of sampling. Please note that although we acknowledge the parallel field of research in tackling inverse problems without backpropagation [25, 45], we excluded these methods for comparison as they tackle solely Linear inverse problems. In contrast, loss-guided models are generic and applicable to a wider range of problems.

5.1 Implementation Details

We perform all experiments on NVIDIA A6000 GPUs. For ImageNet [12] based tasks, we utilize the unconditional model released by Guided Diffusion. For Linear Tasks involving faces, we use the model trained on the FFHQ dataset [23] and perform experiments on the CelebA dataset [26] similar to DPS. For non-linear tasks, we follow Freedom and utilize the model trained unconditionally on the CelebA dataset. We evaluate using conditions derived from existing networks. For the high-resolution results presented in Figure 2, we utilized the class-conditional model of resolution 512×512 released by Guided Diffusion. For all experiments, we used 100 sampling steps. For style transfer, we utilized Stable Diffusion [34] v1.5. Please note that our sampling method is generic, and any sampler can be used. For our experiments, we rescaled the DDPM schedule. We fix the number of augmentations in DiffuseAugment for all the experiments to 8.

5.2 Benchmarks for Linear Inverse Functions

For linear inverse functions, we evaluate four different tasks. For inpainting, we choose a random box mask of width 128×128 pixels. For the Gaussian deblurring task, we apply a 61×61 sized Gaussian blur with kernel intensity 3.0. For super-resolution, we downsample the images using bicubic downsampling to a resolution of 64×64 . For Colorization, we convert to the YCbCr domain and take the Y component as the measurement. As for the choice of comparison methods, we compare two existing methods of loss-guided diffusion: DPS [9] and MGD [17]. The implementation of MGD is based on the parameters mentioned in the original paper. Specifically, a guidance scale of 100 is taken for all linear tasks along with the manifold projection. We also evaluate the method using the Score-SDE method [28]. For super-resolution, we utilize a zero-shot guidance method ILVR [7]. For the choice of metrics, since the linear inverse tasks are image restoration problems, we utilize standard metrics in restoration, namely PSNR and SSIM. We evaluate with LPIPS [52] to measure the perceptual quality of the generated images. To see how close the generated images are to the dataset, we also

Method	Inpaint (Box)				Colorization				SR ($\times 4$)				Gaussian Deblur			
	PSNR \uparrow	SSIM \uparrow	LPIPS \downarrow	FID \downarrow	Cons \uparrow	SSIM \uparrow	LPIPS \downarrow	FID \downarrow	PSNR \uparrow	SSIM \uparrow	LPIPS \downarrow	FID \downarrow	PSNR \uparrow	SSIM \uparrow	LPIPS \downarrow	FID \downarrow
Score-SIDE [43]	9.57	0.329	0.634	94.33	0.1627	0.3996	0.6609	118.86	20.75	0.5844	0.3851	53.22	23.39	0.632	0.361	66.81
ILVR [43]	-	-	-	-	-	-	-	-	26.14	0.7403	0.2776	52.82	-	-	-	-
DPS [8]	19.39	0.610	0.3766	58.89	0.0069	0.5404	0.5594	55.61	17.36	0.4960	0.4613	56.08	20.52	0.5824	0.3756	52.64
MGD [8]	27.21	0.7460	0.2197	11.83	0.0018	0.6865	0.4549	38.22	27.51	0.7852	0.2464	60.21	27.23	0.7695	0.2327	51.59
Ours	28.84	0.8491	0.1432	5.96	0.0014	0.7775	0.3036	20.89	29.47	0.8429	0.1757	46.95	27.30	0.7672	0.2202	42.70

Table 2: Quantitative evaluation of image restoration tasks on CelebA 256 \times 256-1k with $\sigma_y = 0.05$, We utilize 100 inference steps for all methods

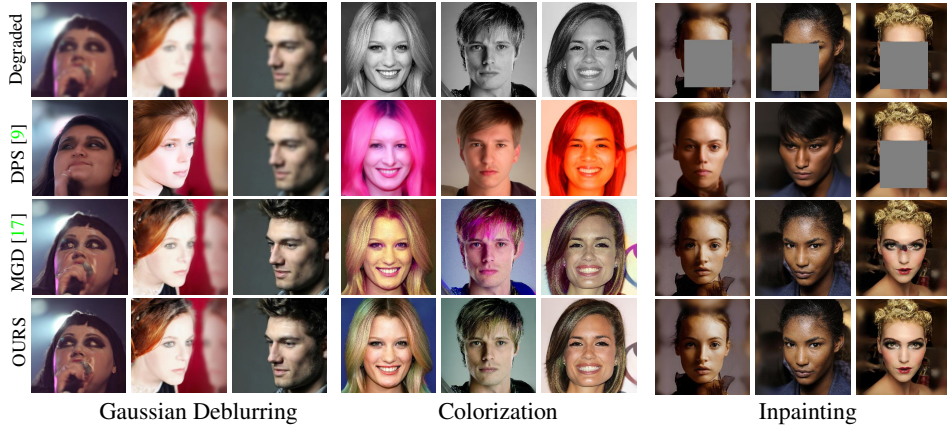


Fig. 3: Qualitative comparisons for Linear Tasks on CelebA dataset for 100 inference steps

evaluate using FID [37]. For the task of colorization, we also evaluate the consistency measure, which denotes the mean square error between the grayscale versions of the reconstructed image and the original image. The lower this score, the better.

5.3 Benchmarks for Non-Linear Inverse Functions

For non-linear inverse functions, we evaluate three different tasks, namely, face parse guidance, face ID guidance, and face sketch guidance. We utilize 1000 images from the CelebA dataset [26] like Freedom [50] and obtain the corresponding non-linear map for each image. For deriving the sketches, we utilize an open-source pre-trained network that converts faces to sketches [48]. For the choice of guidance function, we utilize the Euclidean distance of the generated sketch from the MMSE estimate at each timestep \hat{x}_t . For face parse guidance, we utilize BiSeNet [49] and derive the parse maps from the MMSE estimate at each timestep. We utilize the Euclidean distance between the predicted and ground truth labels as the guidance loss. For face ID guidance, we utilize [13] and get face embeddings corresponding to the images and measure the cosine similarity loss as the guidance function. Please note that for all non-linear tasks, we follow the same setting as in MGD [17] and utilize three-time travel sampling [27] steps. Even though we are performing time travel sampling, our overall compute time is comparable to Freedom because of the time gained by bypassing backpropagation through the UNet. We provide more analysis in the supplementary material. We compare the performance with Freedom [50] (First-order). Here, first-order means the method

Method	Inpaint (Box)			Colorization			SR ($\times 4$)			Gaussian Deblur		
	PSNR \uparrow	SSIM \uparrow	LPIPS \downarrow	FID \downarrow	Cons \uparrow	SSIM \uparrow	LPIPS \downarrow	FID \downarrow	PSNR \uparrow	SSIM \uparrow	LPIPS \downarrow	FID \downarrow
Score-SDE [43]	9.66	0.2087	0.7375	133.54	0.1723	0.3105	0.8197	194.87	14.07	0.2468	0.6766	129.91
ILVR [43]	-	-	-	-	-	-	-	-	15.51	0.4033	0.5253	64.13
DPS [8]	15.23	0.4261	0.6087	97.90	0.021	0.3774	0.8011	106.25	14.94	0.3258	0.6594	87.26
MGD [8]	21.94	0.6920	0.2410	40.30	0.0057	0.5809	0.5427	73.75	23.12	0.6025	0.3936	70.83
Ours	23.49	0.7271	0.2001	30.72	0.0055	0.6804	0.3362	52.76	24.23	0.6818	0.2884	43.00
									23.31	0.6157	0.3566	58.38

Table 3: Quantitative evaluation of image restoration tasks on ImageNet 256 \times 256-1k with $\sigma_y = 0.05$. **Bold:** best, We utilize 100 inference steps for all methods

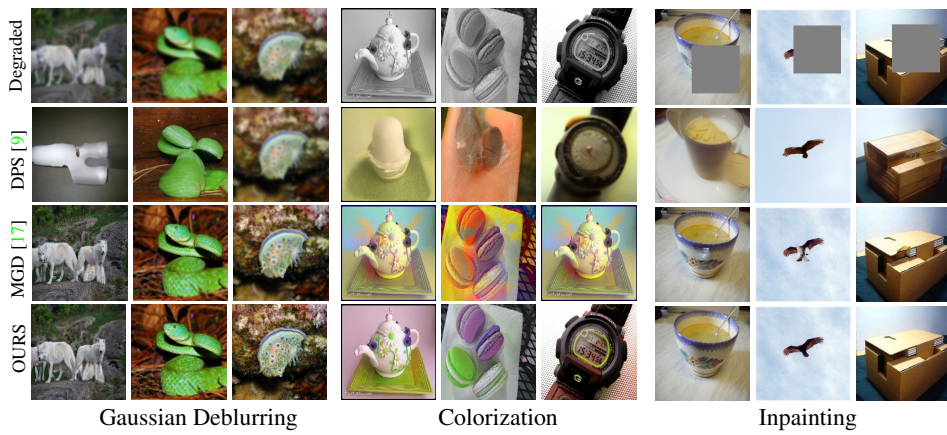


Fig. 4: Qualitative comparisons for Linear Tasks on ImageNet for 100 inference steps

requires backpropagation through the diffusion UNet. We also compare with MGD [17]. For non-linear tasks, we additionally perform a gradient clipping in the range $(-0.2, 0.2)$.

5.4 Qualitative Analysis on Linear Tasks

The qualitative results on faces are given in Figure 3. We present results on Gaussian Deblurring, super-resolution, and colorization. As we can see, DPS fails since 100 steps of diffusion are used, and the DPS scaling factor is not strong enough to perform proper guidance within 100 steps of diffusion. We set the amount of posterior noise for the measurement as 0.05 in all experiments. MGD works remarkably well for the deblurring and inpainting tasks; however, it fails for colorization since early guidance is required for the flow of natural colors. In contrast, our method is able to generate much more natural images for all cases, including colorization, due to the proper flow of gradients at all timesteps. In general, restorative tasks on faces are easier since the domain of images is limited. Hence, we present the results on the ImageNet dataset in Figure 4. For ImageNet tasks, the performance of DPS falls more because the problem is more ill-posed. This can be seen in the eagle diagram, where the method is unable to reconstruct the eagle properly. In contrast, our method performs relatively better, producing much more realistic images. We highlight the performance improvement on colorization since we argue that these results are obtained because of the early flow of gradients. For fair evaluations and measuring the general capability of the comparison algorithm while

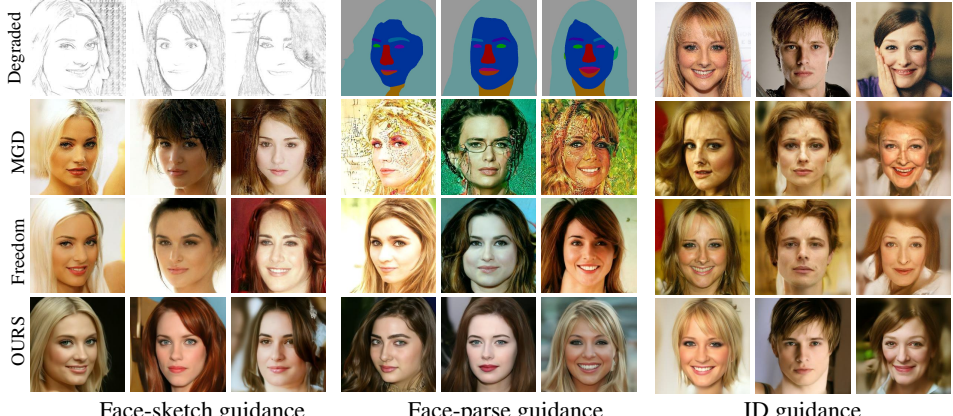


Fig. 5: Qualitative comparisons for Non-linear Tasks on CelebA dataset for 100 inference steps

Method	Semantic Parsing			ID Guidance			Face Sketch		
	Distance↓	LPIPS↓	FID↓	Distance↓	LPIPS↓	FID↓	Distance↓	LPIPS↓	FID↓
<i>First-order</i>									
Freedom [50]	1864.51	0.6030	66.89	0.3767	0.7058	81.40	39.05	0.6583	86.51
<i>Zeroth-order</i>									
MGD [17]	2698.27	0.6995	104.32	0.4291	0.7178	92.61	39.34	0.6576	70.42
Ours	2722.51	0.6199	79.42	0.3780	0.5932	82.70	39.03	0.5509	69.51

Table 4: Non-linear tasks. Best results out of zeroth-order optimization algorithms are highlighted.

evaluating on Face Datasets, we utilize the model trained on the FFHQ dataset [23] and test on the CelebA dataset [26]. For ImageNet-related experiments, we evaluate the ImageNet validation set.

5.5 Quantitative Analysis on Linear Tasks

As mentioned in Section 5.2, we utilize Dreamguider and quantitatively evaluate CelebA and ImageNet datasets. The results for face restoration tasks are shown in Table 2 and Table 3. We evaluate these tasks utilizing four different metrics. SDEdit [28] fails for the task of face inpainting and colorization as a single perturbation in the noisy domain throws the image off the manifold. DPS requires more inference steps for proper guidance. ILVR is originally designed for super-resolution. Hence, we quantitatively evaluate ILVR [7] only for the task of super-resolution. Since DPS and MGD are applicable to all cases, we evaluate with these methods. As we can see, our approach obtains better results than the baselines because of the flow of gradients, which allows for better reconstruction quality. For faces, the difference is much more highlighted in the task of colorization, where we get a significant boost of 18 FID score above the baseline. General linear inverse problems in ImageNet are much more complex than in faces; hence, there is an overall drop in metrics for the natural domain images in ImageNet.

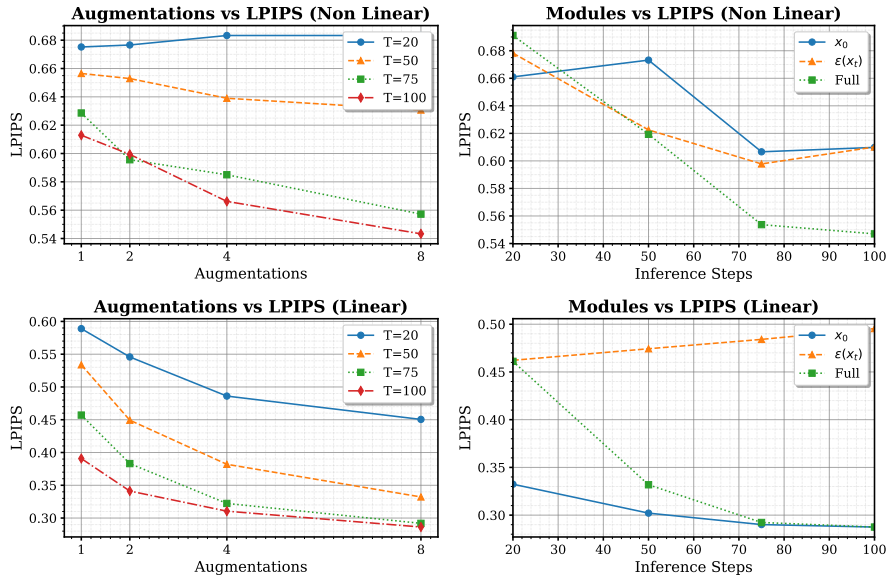


Fig. 6: Ablation analysis on linear and non-linear tasks. **Top Row:** FaceID guidance **Bottom Row:** ImageNet superresolution

5.6 Analysis on Non-Linear Tasks

As mentioned in Section 5.3, we evaluate our method with the existing methods Freedom [50] and MGD [17]. Figure 5 presents the corresponding qualitative results. As we can see, Freedom is able to produce realistic-looking results for even the difficult task of Parse Maps to Faces. We argue that this is because backpropagation through the UNet purifies the gradient flow; hence, the generated images look much more naturalistic. In our case, DiffAugment purifies the gradient; hence, we look for much better realistic-looking images. However, MGD does not produce realistic results for sketch-to-image synthesis and anime-to-face synthesis. We evaluate the methods in terms of Distance, which is the measure of the L_2 norm between the generated degradation maps and their original maps. Also, to measure the perceptual quality, we utilize the LPIPS score as well as the FID score. One point to note here is that even though there are artifacts in the generated images in MGD, this is not accurately reflected in the metrics. The corresponding metrics are presented in Section 5.5. As we can see, compared to the first-order cases, we obtained better metrics in terms of FID and LPIPS in all the cases. In some cases, our value is lower than that of Freedom; however, the compute time is much lower than Freedom, hence being the tradeoff.

6 Ablation Studies

We perform extensive ablation studies with respect to the effect of DiffuseAugment as well as the effect of each guidance term. For the ablation experiments, rather than

utilizing the whole testing dataset of 1000 images, because of the bulk of the number of experiments, we utilize 100 images and report the average LPIPS value.

6.1 Effect of DiffuseAugment

To analyze the effect of DiffuseAugment, we experiment with different values for augmentation numbers for both linear and non-linear tasks. For the choice of linear task, we choose ImageNet Super-resolution ($\times 4$). We first vary the number of diffusion sampling steps from 20, 50, 75, 100 and measure the average LPIPS score across all images to measure the overall perceptual quality. We notice that for linear tasks, even for low values of T such as $T = 20$, just by increasing the number of augmentations at the output to 8, the perceptual quality drastically improves, matching that of diffusion inference with $T = 50$ with just 2 augmentations. Further, we notice that although the effect of augmentations is very significant for linear tasks, the performance is not that significant or rather drops in some cases for low T such as $T = 20$; this is because with 20 diffusion steps, most intermediate MMSE estimates remain noisy, and hence the guidance network ArcFace [13] cannot handle such input and hence returns irregular gradients affecting the quality. However, we can see that as T increases and when there are enough gradient steps, DiffuseAugment plays a significant role in boosting the performance.

6.2 Effect of Different Components of Guidance

We present the ablation analysis of the effect of different terms of guidance in Figure 6. Please note that for this experiment, we set the number of augmentations from DiffuseAugment as 1. We also turn off time travel sampling for this experiment. We can see the performance while guiding with different components mentioned in Section 4. As we can see, guidance with \hat{x}_t alone faces a drop in performance initially for a low number of inference steps. We argue that this is because the guidance flow through the MMSE estimate alone is weak during the earlier steps of diffusion. Although time travel sampling helps to alleviate this issue, careful parameter tuning is required to obtain satisfactory results. We also notice that guiding utilizing the gradients of the output noise of the network ϵ_t produces better results when the number of timesteps is low; however, the effect falls off as the number of steps increases. This is because the effect as the sampling proceeds is only effective in the initial steps. However, in our case, since there is proper guidance during the start as well as the end, the perceptual quality improves. These are also reflected in Section 5.5. The effect of dual descent is more prominent for non-linear inverse problems where the gradient estimate is inaccurate. In the case of linear inverse problems, however, we find that dual descent is not that beneficial and might lead to a small drop in performance, as shown in Figure 6. More examples are provided in the supplementary material.

7 Future Works

Although we illustrated the working across various tasks for pixel space diffusion models, the direct approach cannot be used for latent diffusion models for the task

of linear inverse problems, and one might have to apply multiple steps of time travel sampling to fix this issue, making a large computational overhead of the overall sampling time. We emphasize that this problem arises due to the reconstruction error in the VAE that encodes the image to the latent space. In the future, we will attempt to improve upon this with better optimization techniques. Moreover, although the proposed empirical estimate based on distance over gradients works for most tasks and shows the existence of an optimal parameter estimate, a thorough mathematical evaluation and the most optimal parameters are still missing. We leave this problem up to future works to estimate the optimal guidance parameter.

8 Conclusion

In this paper, we proposed an improvement to existing loss-guided techniques for zero-shot conditional generation with an unconditional diffusion model. Specifically, we proposed a sampling technique that removes the need to backpropagate through the diffusion U-Net in order to tackle sampling for general inverse problems. We also present an empirical function for automatic scaling parameters that removes the need for manual scaling parameter tuning, which was previously a huge hurdle in using classifier-free guidance. The newly proposed scaling parameter also removes the need for model-specific tuning of start and end guidance steps. We also introduced a differentiable data augmentation method that significantly improves the sampling fidelity. We illustrated the working of our method across 4 linear and 3 non-linear tasks across faces and real image domains. Our sampling technique produces photorealistic samples with much lower sampling time and higher fidelity than existing methods.

References

1. Aggarwal, H.K., Mani, M.P., Jacob, M.: MoDL: Model-based deep learning architecture for inverse problems. *IEEE transactions on medical imaging* **38**(2), 394–405 (2018) [4](#)
2. Arjovsky, M., Chintala, S., Bottou, L.: Wasserstein generative adversarial networks. In: International conference on machine learning. pp. 214–223. PMLR (2017) [2](#)
3. Balaji, Y., Nah, S., Huang, X., Vahdat, A., Song, J., Kreis, K., Aittala, M., Aila, T., Laine, S., Catanzaro, B., et al.: ediffi: Text-to-image diffusion models with an ensemble of expert denoisers. arXiv preprint arXiv:2211.01324 (2022) [2](#)
4. Bansal, A., Chu, H.M., Schwarzschild, A., Sengupta, S., Goldblum, M., Geiping, J., Goldstein, T.: Universal guidance for diffusion models. arXiv preprint arXiv:2302.07121 (2023) [2, 4](#)
5. Blattmann, A., Rombach, R., Ling, H., Dockhorn, T., Kim, S.W., Fidler, S., Kreis, K.: Align your latents: High-resolution video synthesis with latent diffusion models. In: Proceedings of the IEEE/CVF Conference on Computer Vision and Pattern Recognition. pp. 22563–22575 (2023) [2](#)
6. Chan, S.H., Wang, X., Elgendi, O.A.: Plug-and-play admm for image restoration: Fixed-point convergence and applications. *IEEE Transactions on Computational Imaging* **3**(1), 84–98 (2016) [2](#)
7. Choi, J., Kim, S., Jeong, Y., Gwon, Y., Yoon, S.: Ilvr: Conditioning method for denoising diffusion probabilistic models. arXiv preprint arXiv:2108.02938 (2021) [9, 12](#)

8. Chung, H., Kim, J., Mccann, M.T., Klasky, M.L., Ye, J.C.: Diffusion posterior sampling for general noisy inverse problems. In: International Conference on Learning Representations (2023), <https://openreview.net/forum?id=OnD9zGAGT0k> 2, 5, 10, 11
9. Chung, H., Ryu, D., Mccann, M.T., Klasky, M.L., Ye, J.C.: Solving 3d inverse problems using pre-trained 2d diffusion models. IEEE/CVF Conference on Computer Vision and Pattern Recognition (2023) 2, 3, 4, 5, 8, 9, 10, 11
10. Chung, H., Ye, J.C., Milanfar, P., Delbracio, M.: Prompt-tuning latent diffusion models for inverse problems. ArXiv [abs/2310.01110](https://arxiv.org/abs/2310.01110) (2023) 4
11. Defazio, A., Mishchenko, K.: Learning-rate-free learning by d-adaptation. arXiv preprint arXiv:2301.07733 (2023) 3
12. Deng, J., Dong, W., Socher, R., Li, L.J., Li, K., Fei-Fei, L.: Imagenet: A large-scale hierarchical image database. In: 2009 IEEE conference on computer vision and pattern recognition. pp. 248–255. Ieee (2009) 9
13. Deng, J., Guo, J., Xue, N., Zafeiriou, S.: Arcface: Additive angular margin loss for deep face recognition. In: Proceedings of the IEEE/CVF conference on computer vision and pattern recognition. pp. 4690–4699 (2019) 10, 14
14. Dhariwal, P., Nichol, A.: Diffusion models beat gans on image synthesis. Advances in Neural Information Processing Systems **34** (2021) 2, 6
15. Goodfellow, I., Pouget-Abadie, J., Mirza, M., Xu, B., Warde-Farley, D., Ozair, S., Courville, A., Bengio, Y.: Generative adversarial networks. Communications of the ACM **63**(11), 139–144 (2020) 2
16. Graikos, A., Malkin, N., Jojic, N., Samaras, D.: Diffusion models as plug-and-play priors. arXiv preprint arXiv:2206.09012 (2022) 2
17. He, Y., Murata, N., Lai, C.H., Takida, Y., Uesaka, T., Kim, D., Liao, W.H., Mitsufuji, Y., Kolter, J.Z., Salakhutdinov, R., et al.: Manifold preserving guided diffusion. arXiv preprint arXiv:2311.16424 (2023) 3, 4, 5, 7, 9, 10, 11, 12, 13
18. Ho, J., Chan, W., Saharia, C., Whang, J., Gao, R., Gritsenko, A., Kingma, D.P., Poole, B., Norouzi, M., Fleet, D.J., et al.: Imagen video: High definition video generation with diffusion models. arXiv preprint arXiv:2210.02303 (2022) 2
19. Ho, J., Jain, A., Abbeel, P.: Denoising diffusion probabilistic models. Advances in Neural Information Processing Systems **33**, 6840–6851 (2020) 2
20. Hossain, M.Z., Sohel, F., Shiratuddin, M.F., Laga, H.: A comprehensive survey of deep learning for image captioning. ACM Computing Surveys (CsUR) **51**(6), 1–36 (2019) 2
21. Ivgi, M., Hinder, O., Carmon, Y.: Dog is sgd’s best friend: A parameter-free dynamic step size schedule. arXiv preprint arXiv:2302.12022 (2023) 3, 8
22. Jun, H., Nichol, A.: Shap-e: Generating conditional 3d implicit functions. arXiv preprint arXiv:2305.02463 (2023) 2
23. Karras, T., Aila, T., Laine, S., Lehtinen, J.: Progressive growing of GANs for improved quality, stability, and variation. arXiv preprint arXiv:1710.10196 (2017) 9, 12
24. Kawar, B., Elad, M., Ermon, S., Song, J.: Denoising diffusion restoration models. arXiv preprint arXiv:2201.11793 (2022) 4
25. Kawar, B., Vaksman, G., Elad, M.: Stochastic image denoising by sampling from the posterior distribution. In: Proceedings of the IEEE/CVF International Conference on Computer Vision (ICCV) Workshops. pp. 1866–1875 (October 2021) 9
26. Liu, Z., Luo, P., Wang, X., Tang, X.: Deep learning face attributes in the wild. In: Proceedings of International Conference on Computer Vision (ICCV) (December 2015) 9, 10, 12
27. Lugmayr, A., Danelljan, M., Romero, A., Yu, F., Timofte, R., Van Gool, L.: Repaint: Inpainting using denoising diffusion probabilistic models. In: Proceedings of the IEEE/CVF Conference on Computer Vision and Pattern Recognition. pp. 11461–11471 (2022) 10, 20
28. Meng, C., Song, Y., Song, J., Wu, J., Zhu, J.Y., Ermon, S.: SDEdit: Image synthesis and editing with stochastic differential equations. arXiv preprint arXiv:2108.01073 (2021) 9, 12

29. Nair, N.G., Cherian, A., Lohit, S., Wang, Y., Koike-Akino, T., Patel, V.M., Marks, T.K.: Steered diffusion: A generalized framework for plug-and-play conditional image synthesis. In: Proceedings of the IEEE/CVF International Conference on Computer Vision. pp. 20850–20860 (2023) [2](#), [3](#), [4](#), [5](#)
30. Nguyen, A., Clune, J., Bengio, Y., Dosovitskiy, A., Yosinski, J.: Plug & play generative networks: Conditional iterative generation of images in latent space. In: Proceedings of the IEEE conference on computer vision and pattern recognition. pp. 4467–4477 (2017) [2](#)
31. Nichol, A.Q., Dhariwal, P.: Improved denoising diffusion probabilistic models. In: International Conference on Machine Learning. pp. 8162–8171. PMLR (2021) [3](#)
32. Poole, B., Jain, A., Barron, J.T., Mildenhall, B.: Dreamfusion: Text-to-3d using 2d diffusion. arXiv (2022) [2](#)
33. Radford, A., Metz, L., Chintala, S.: Unsupervised representation learning with deep convolutional generative adversarial networks. arXiv preprint arXiv:1511.06434 (2015) [2](#)
34. Rombach, R., Blattmann, A., Lorenz, D., Esser, P., Ommer, B.: High-resolution image synthesis with latent diffusion models (2021) [2](#), [3](#), [9](#)
35. Saharia, C., Chan, W., Chang, H., Lee, C., Ho, J., Salimans, T., Fleet, D., Norouzi, M.: Palette: Image-to-image diffusion models. In: ACM SIGGRAPH 2022 Conference Proceedings. pp. 1–10 (2022) [2](#)
36. Saharia, C., Ho, J., Chan, W., Salimans, T., Fleet, D.J., Norouzi, M.: Image super-resolution via iterative refinement. IEEE Transactions on Pattern Analysis and Machine Intelligence (2022) [2](#)
37. Seitzer, M.: pytorch-fid: FID Score for PyTorch. <https://github.com/mseitzer/pytorch-fid> (August 2020), version 0.3.0 [10](#)
38. Simonyan, K., Zisserman, A.: Very deep convolutional networks for large-scale image recognition. arXiv preprint arXiv:1409.1556 (2014) [2](#)
39. Sohl-Dickstein, J., Weiss, E., Maheswaranathan, N., Ganguli, S.: Deep unsupervised learning using nonequilibrium thermodynamics. In: International Conference on Machine Learning. pp. 2256–2265. PMLR (2015) [2](#), [5](#), [20](#)
40. Song, J., Meng, C., Ermon, S.: Denoising diffusion implicit models. In: 9th International Conference on Learning Representations, ICLR (2021) [7](#)
41. Song, J., Vahdat, A., Mardani, M., Kautz, J.: Pseudoinverse-guided diffusion models for inverse problems. In: International Conference on Learning Representations (2022) [5](#)
42. Song, J., Zhang, Q., Yin, H., Mardani, M., Liu, M.Y., Kautz, J., Chen, Y., Vahdat, A.: Loss-guided diffusion models for plug-and-play controllable generation. In: International Conference on Machine Learning. pp. 32483–32498. PMLR (2023) [3](#)
43. Song, Y., Sohl-Dickstein, J., Kingma, D.P., Kumar, A., Ermon, S., Poole, B.: Score-based generative modeling through stochastic differential equations. In: International Conference on Learning Representations (2021), <https://openreview.net/forum?id=PxTIG12RRHS> [2](#), [10](#), [11](#)
44. Wang, T.C., Liu, M.Y., Zhu, J.Y., Tao, A., Kautz, J., Catanzaro, B.: High-resolution image synthesis and semantic manipulation with conditional gans. In: Proceedings of the IEEE conference on computer vision and pattern recognition. pp. 8798–8807 (2018) [2](#)
45. Wang, Y., Yu, J., Zhang, J.: Zero-shot image restoration using denoising diffusion null-space model. In: The Eleventh International Conference on Learning Representations (2023), <https://openreview.net/forum?id=mRieQgMtNTQ> [9](#)
46. Wu, J.Z., Ge, Y., Wang, X., Lei, S.W., Gu, Y., Shi, Y., Hsu, W., Shan, Y., Qie, X., Shou, M.Z.: Tune-a-video: One-shot tuning of image diffusion models for text-to-video generation. In: Proceedings of the IEEE/CVF International Conference on Computer Vision. pp. 7623–7633 (2023) [2](#)
47. Wu, Z., Zhou, P., Kawaguchi, K., Zhang, H.: Fast diffusion model. arXiv preprint arXiv:2306.06991 (2023) [8](#)

48. Xiang, X., Liu, D., Yang, X., Zhu, Y., Shen, X., Allebach, J.P.: Adversarial open domain adaptation for sketch-to-photo synthesis. In: Proceedings of the IEEE/CVF Winter Conference on Applications of Computer Vision. pp. 1434–1444 (2022) [10](#)
49. Yu, C., Wang, J., Peng, C., Gao, C., Yu, G., Sang, N.: Bisenet: Bilateral segmentation network for real-time semantic segmentation. In: Proceedings of the European conference on computer vision (ECCV). pp. 325–341 (2018) [10](#)
50. Yu, J., Wang, Y., Zhao, C., Ghanem, B., Zhang, J.: Freedom: Training-free energy-guided conditional diffusion model. arXiv preprint arXiv:2303.09833 (2023) [2](#), [3](#), [4](#), [5](#), [10](#), [12](#), [13](#), [20](#)
51. Zhang, K., Li, Y., Zuo, W., Zhang, L., Van Gool, L., Timofte, R.: Plug-and-play image restoration with deep denoiser prior. IEEE Transactions on Pattern Analysis and Machine Intelligence **44**(10), 6360–6376 (2021) [7](#)
52. Zhang, R., Isola, P., Efros, A.A., Shechtman, E., Wang, O.: The unreasonable effectiveness of deep features as a perceptual metric. In: CVPR (2018) [9](#)
53. Zhao, S., Liu, Z., Lin, J., Zhu, J.Y., Han, S.: Differentiable augmentation for data-efficient gan training. Advances in neural information processing systems **33**, 7559–7570 (2020) [3](#)

Supplementary Material: Dreamguider: Double Descent Guided Diffusion

Nithin Gopalakrishnan Nair^{ID} and Vishal M Patel

Johns Hopkins University, Baltimore, Maryland 21218

{ngopala2, vpatel36}@jhu.edu

<http://www.springer.com/gp/computer-science/lncs>

1 Algorithm of Dreamguider

We present the over algorithm of dreamguider without time travel sampling and the parameter estimation algorithm in Algorithm 1

Algorithm 1 Dreamguider

Input: distance function $r(\cdot, y)$, condition y , Timesteps T

- 1: $x_T \sim \mathcal{N}(x_T; 0, I)$
- 2: **for** $t = T - 1, \dots, 1$ **do**
- 3: $\Sigma = \sqrt{1 - \bar{\alpha}_t}$
- 4: $\epsilon \sim \mathcal{N}(\epsilon; 0, I)$
- 5: $\hat{x}_t = \frac{x_t - \sqrt{1 - \bar{\alpha}_t} \epsilon_\theta(x_t)}{\sqrt{\bar{\alpha}_t}}$
- 6: Compute $\frac{dr(\hat{x}_t, y)}{d\hat{x}_t}, \frac{dr(\hat{x}_t, y)}{d\epsilon_\theta(x_t)}$
- 7: update $c = ESTIMATE(t, \epsilon_\theta(x_t), \frac{dr(\hat{x}_t, y)}{d\epsilon_\theta(x_t)})$
- 8: update $d = ESTIMATE(t, \hat{x}_t, \frac{dr(\hat{x}_t, y)}{d\hat{x}_t})$
- 9: $c_t = c \sqrt{\alpha_{t-1}}$
- 10: $d_t = -d \frac{1 - \alpha_t}{\sqrt{\alpha_t} \sqrt{1 - \alpha_t}}$
- 11: $x_{t-1} = \frac{1}{\sqrt{\alpha_t}} \left(x_t - \frac{1 - \alpha_t}{\sqrt{1 - \alpha_t}} \epsilon_\theta(x_t) \right) + \sigma_t \epsilon - c_t \Sigma \frac{dr(\hat{x}_t, y)}{d\hat{x}_t} - d_t \Sigma \frac{dr(\hat{x}_t, y)}{d\epsilon_\theta(x_t)}$
- 12: **end for**
- 13: **function** $ESTIMATE(t, f_i, g_t)$
- 14: **if** $t = T$ **then**
- 15: $\gamma_t = \frac{1e^{-5}}{\sqrt{g_T^2}}$
- 16: Store f_T ,
- 17: **else**
- 18: $\gamma_t = \frac{\max i > t |f_i - f_T|}{\sqrt{\sum_{i=t}^T g_i^2}}$
- 19: **end if**
- 20: Store $\sqrt{\sum_{i=t}^T g_i^2}$
- 21: **return** γ_t
- 22: **end function return** x_0

2 Proof for perturbed Markovian kernel equation

In the main paper, we emphasized that any positive distance function can be utilized for performing conditional generation using the perturbed Markovian kernel equation. Here we proceed to derive the perturbed transition step. For the proof we closely follow the work from Dickenson et al [39]. Given a unconditional transition distribution $p_\theta(x_{t-1}|x_t)$ and a distance function $r(., y)$, where y is the condition provided. Please note that we assume $r(., y)$ has relatively small variance compared to $p_\theta(x_{t-1}|x_t)$. We know that at equilibrium state, the distribution at any timestep t in a diffusion model can be written as

$$p(x_{t-1}) = \int p(x_t)p_\theta(x_{t-1}|x_t)dx_t. \quad (1)$$

To estimate a perturbed transition kernel $\hat{p}(x_{t-1}|x_t)$, we start the perturbed distribution as

$$p(x_{t-1})r(x_{t-1}, y) = \int r(x_t, y)p(x_t)\hat{p}_\theta(x_{t-1}|x_t)dx_t. \quad (2)$$

By simple algebraic manipulations, taking $r(x_{t-1}, y)$ to the other side, we get

$$p(x_{t-1}) = \int \frac{r(x_t, y)}{r(x_{t-1}, y)}p(x_t)\hat{p}_\theta(x_{t-1}|x_t)dx_t. \quad (3)$$

By comparing Equation (1) and Equation (3) we can see that one solution for the transitional distribution is

$$\hat{p}_\theta(x_{t-1}|x_t) = p_\theta(x_{t-1}|x_t) \frac{r(x_{t-1}, y)}{r(x_t, y)}. \quad (4)$$

Also since normalization constants doesn't affect the score function or transition step, Absorbing x_t to the normalization factor of $p_\theta(x_{t-1}|x_t)$, another valid perturbed transition kernel is

$$\hat{p}_\theta(x_{t-1}|x_t) = p_\theta(x_{t-1}|x_t) \frac{r(x_{t-1}, y)}{Z}. \quad (5)$$

Please note that the term Z does not affect the transition step in the reverse process when the variance of $r(., y)$ is small.

Method	Freedom	Dreamguider(1)	Dreamguider(2)	Dreamguider(3)
Sketch to Face	24.95	17.55	27.04	35.09
FaceID to Face	24.94	20.45	31.89	41.80
FaceParse to Face	56.25	48.35	75.43	107.02

Table 1: Non-linear tasks ablation analysis on time taken, the value is represented in seconds

3 Time comparison for Dreamguider with timetravel sampling and Freedom(First order) for non linear tasks

We present the time taken by Freedom, a first order algorithm for one step of time travel sampling [27, 50] in Table 1

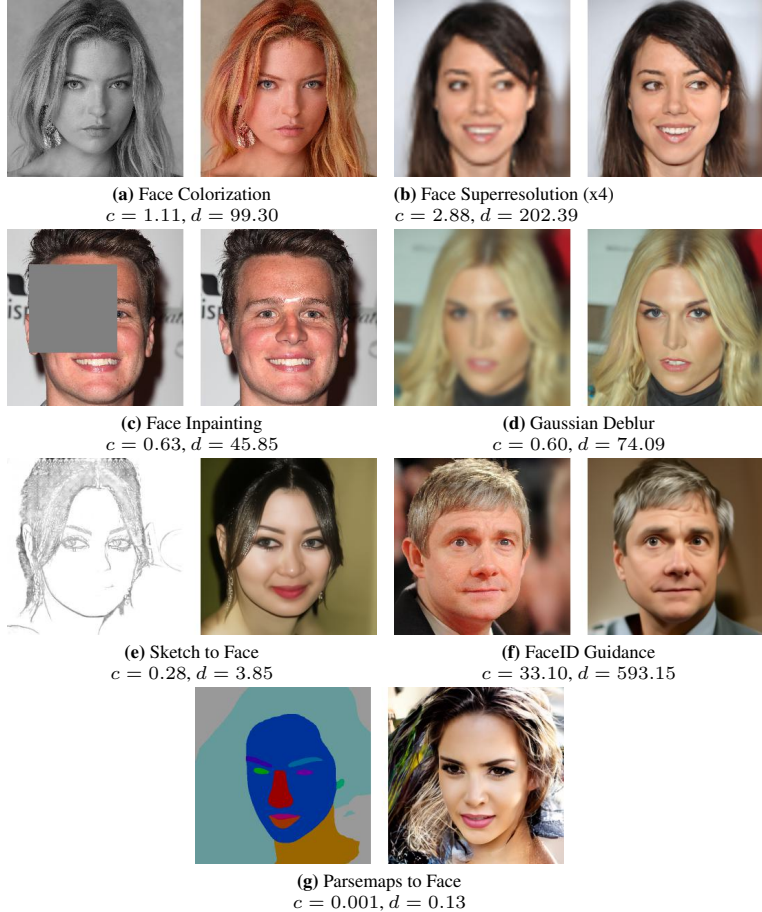


Fig. 1: Figure illustrating the guidance scales for different tasks.

4 Estimated parameter value for different tasks

In this section, we present the result and the parameter estimated by our approach for different tasks. For this experiment, we use 100 timesteps of diffusion and present the value at the 100th timestep. Here we define d as the scaling factor of the scaling constant of the loss derivative relative to $\epsilon_\theta(x_t)$ and c as that of \hat{x}_t as in the main paper . The corresponding results are shown in Figure 1

5 Non cherry picked results for different tasks.

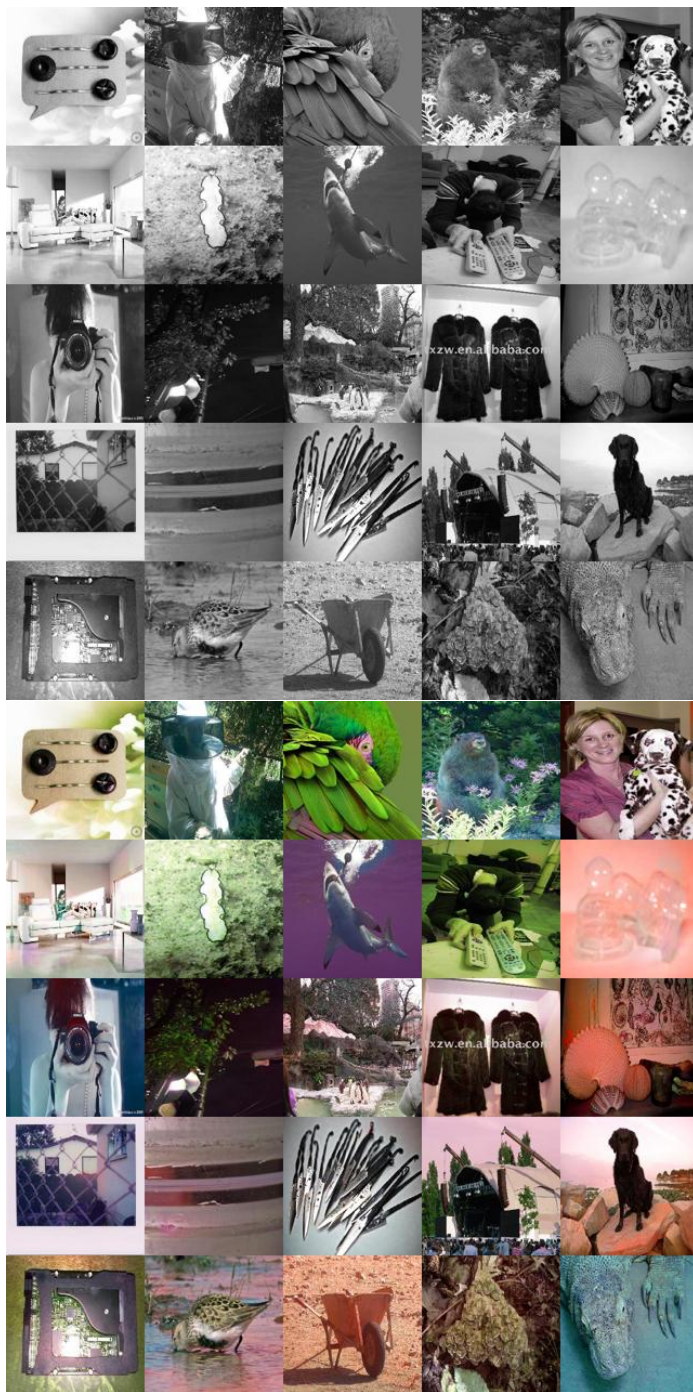


Fig. 2: Figure illustrating **Non cherry picked** results for ImageNet colorization

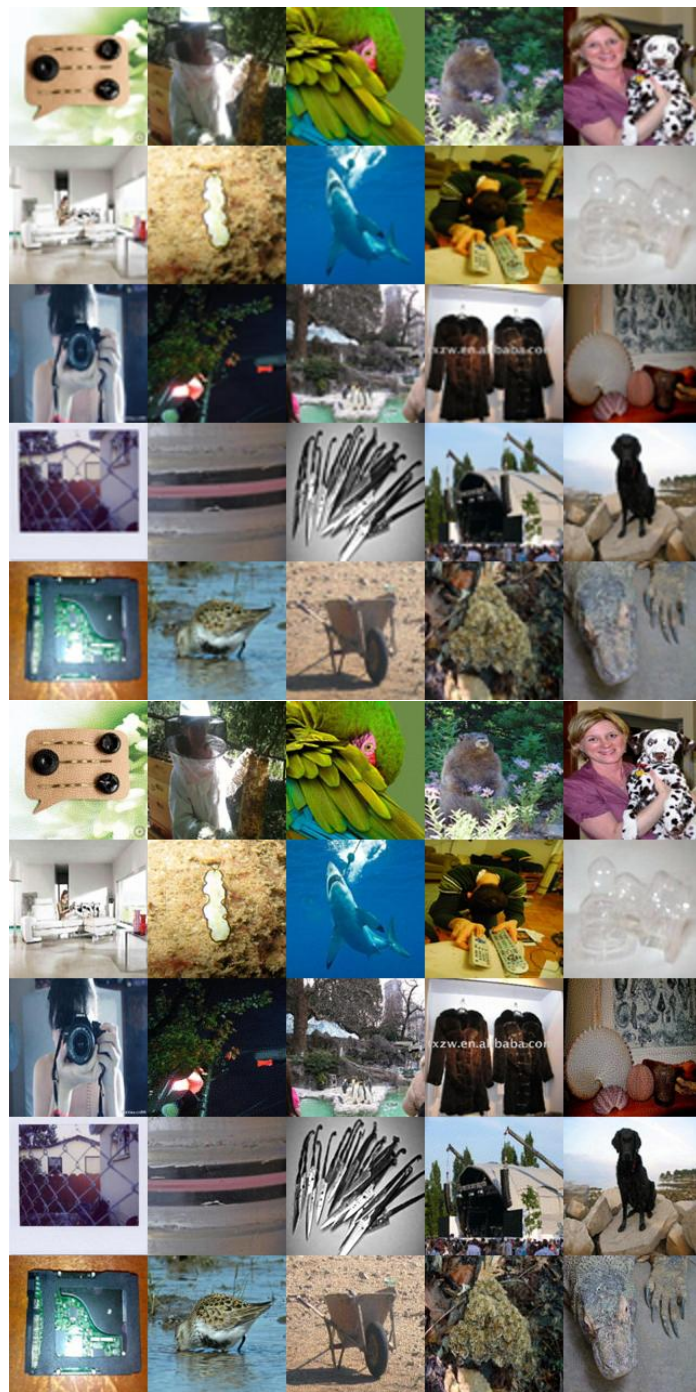


Fig. 3: Figure illustrating Non cherry picked results for ImageNet superresolution

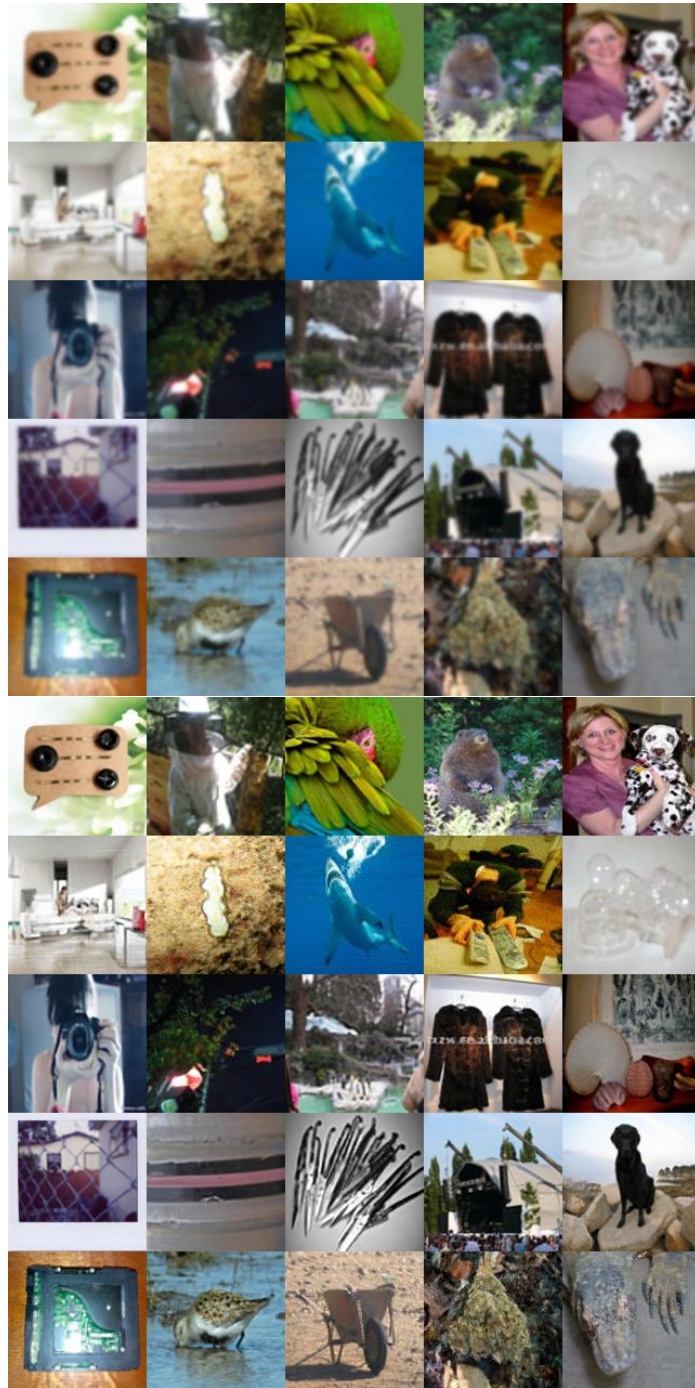


Fig. 4: Figure illustrating **Non cherry picked** results for Gaussian deblurring on ImageNet



Fig. 5: Figure illustrating Non cherry picked results for face colorization

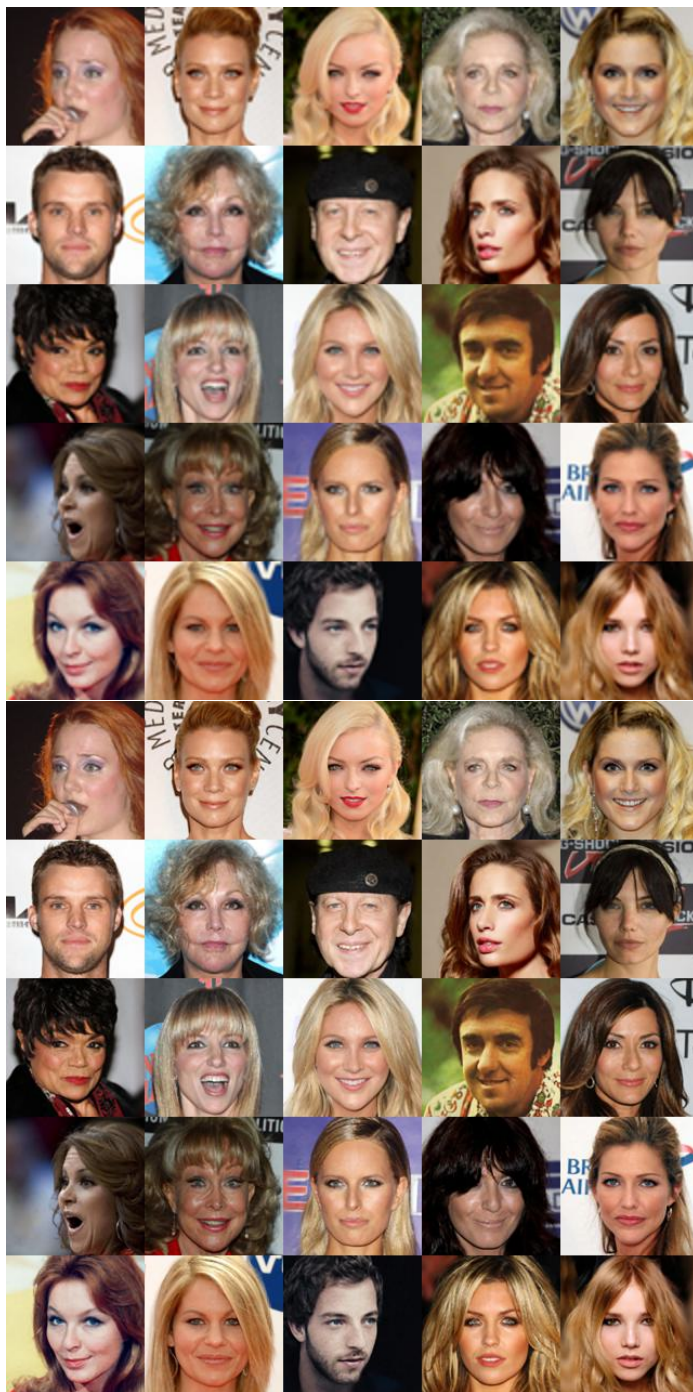


Fig. 6: Figure illustrating **Non cherry picked** results for face superresolution

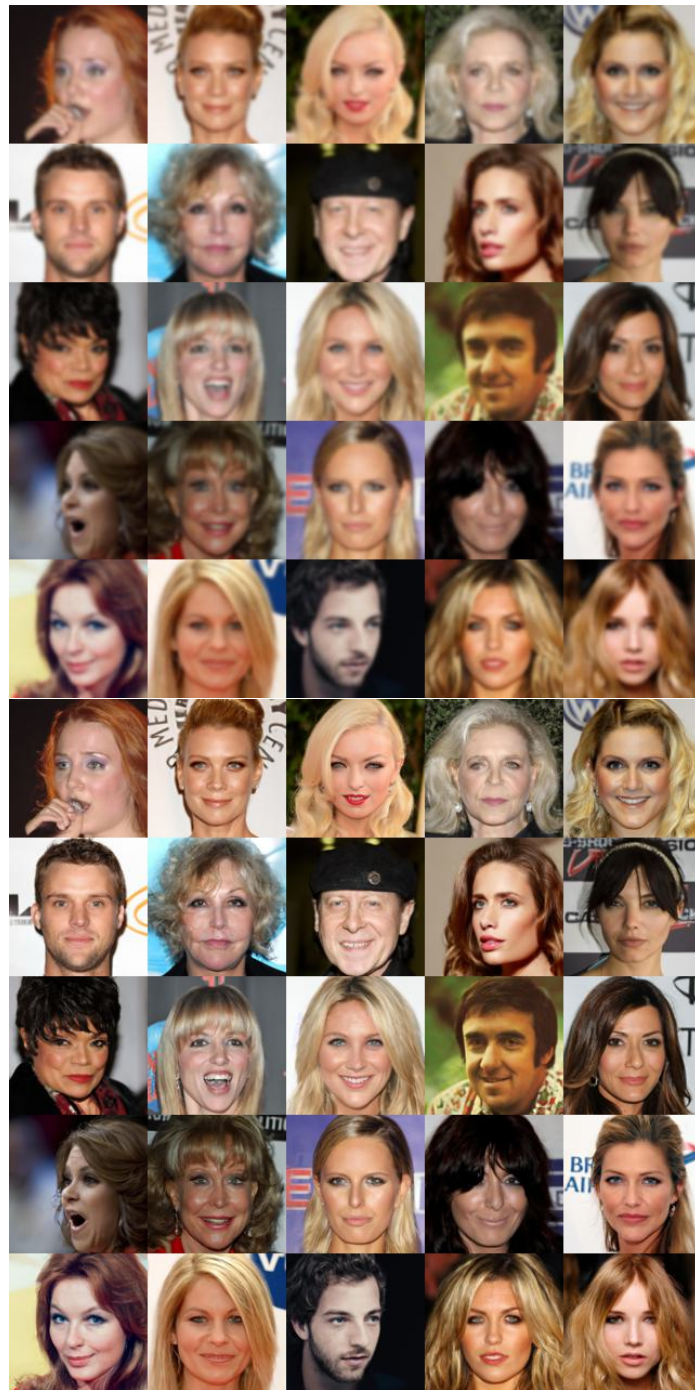


Fig. 7: Figure illustrating **Non cherry picked** results for Gaussian Deblurring



Fig. 8: Figure illustrating **Non cherry picked** results for face inpainting

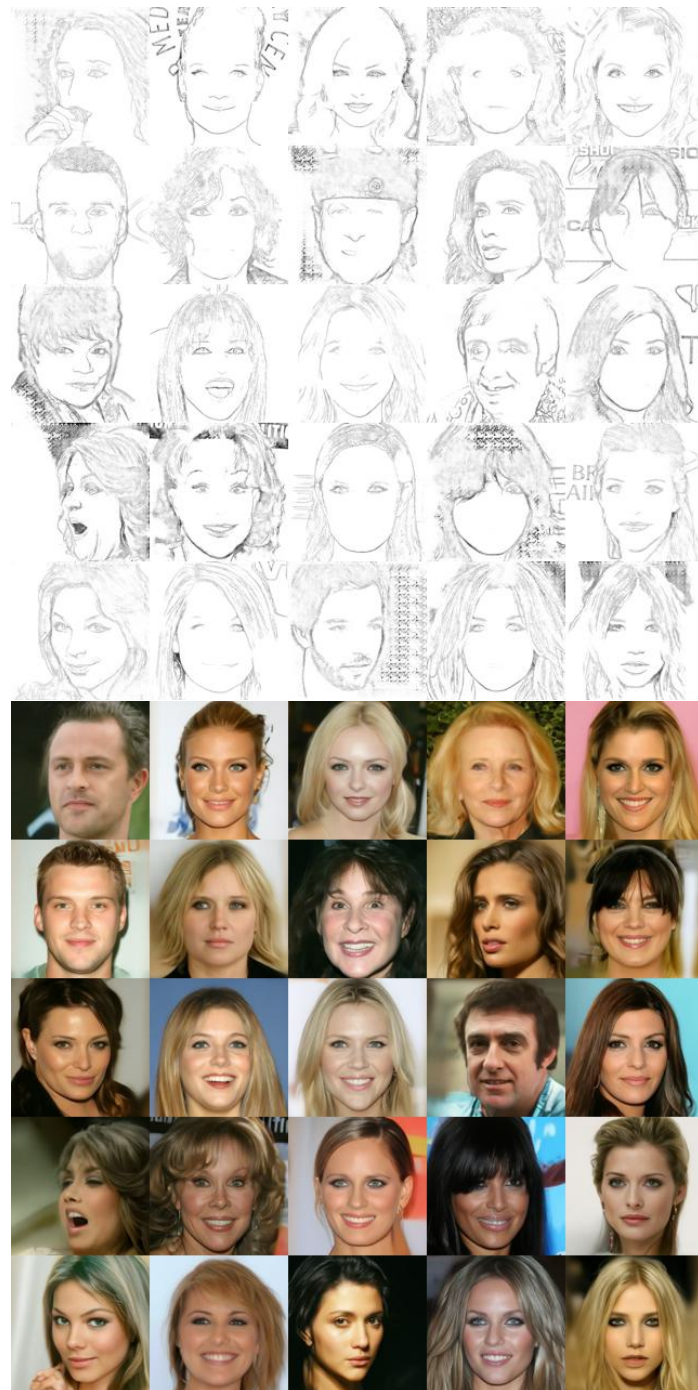


Fig. 9: Figure illustrating **Non cherry picked** results for sketch to face synthesis

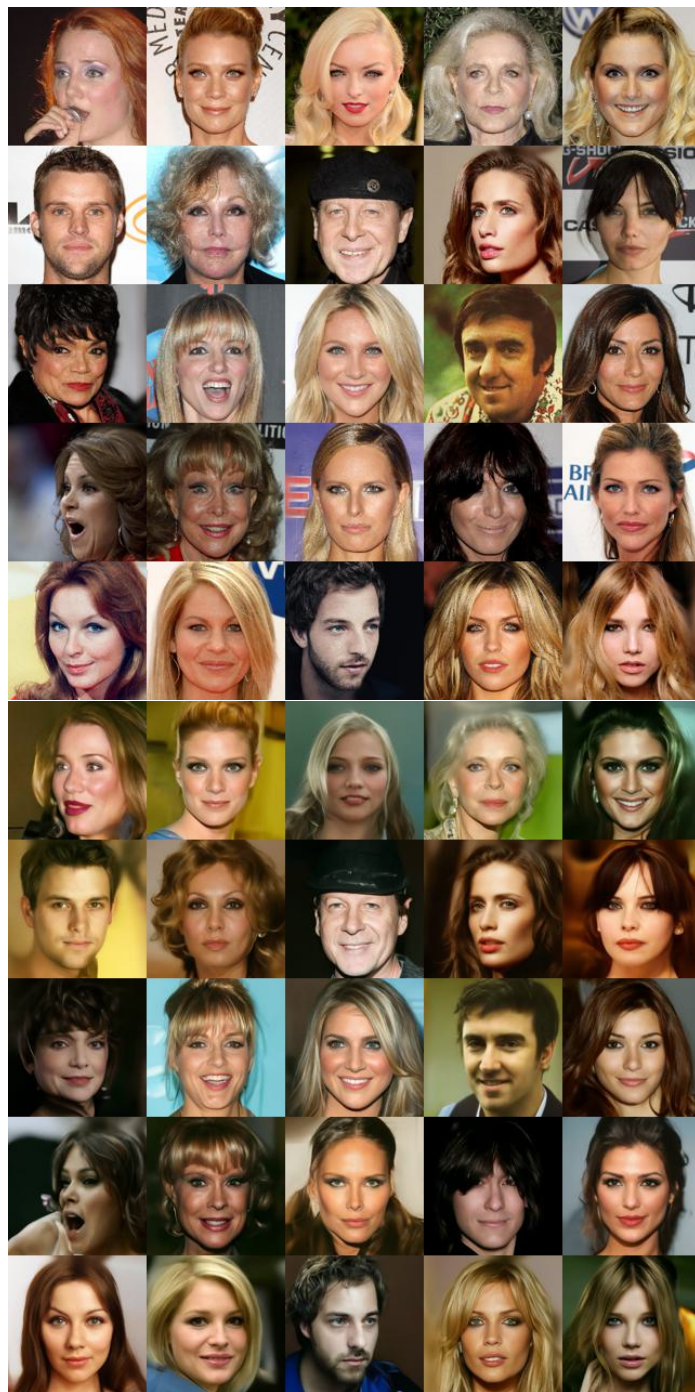


Fig. 10: Figure illustrating **Non cherry picked** results for Face ID guidance



Fig. 11: Figure illustrating **Non cherry picked** results for Face Parse Guidance